

Wigner representation of Andreev-reflected charge pulses

Benjamin Roussel,¹ Pablo Buset,^{2,3,4} and Christian Flindt¹

¹*Department of Applied Physics, Aalto University, 00076 Aalto, Finland*

²*Department of Theoretical Condensed Matter Physics, Universidad Autónoma de Madrid, 28049 Madrid, Spain*

³*Condensed Matter Physics Center (IFIMAC), Universidad Autónoma de Madrid, 28049 Madrid, Spain*

⁴*Instituto Nicolás Cabrera, Universidad Autónoma de Madrid, 28049 Madrid, Spain*

Recent experiments have shown that the edge states of a quantum Hall sample can be coupled to a superconductor, so that incoming electrons in the edge states can be Andreev converted by the superconductor as coherent superpositions of an electron and a hole. In parallel, single-electron emitters that operate in the gigahertz regime have been realized on quantum Hall edge states. Motivated by this remarkable experimental progress, we here analyze the Andreev reflections of incoming charge pulses on the interface with a superconductor. To this end, we employ a Wigner function representation that allows us to visualize the response function of the interface both in the time and in the frequency domain. We analyze the response of an interface between a normal-metal and a singlet or triplet superconductor with and without an insulating barrier in between them. As a special case, we analyze the Andreev reflections of clean single-particle excitations that are generated by the application of lorentzian-shaped voltage pulses to the contacts of the inputs. Our predictions may be tested in future experiments with edge states coupled to superconductors.

I. INTRODUCTION

Electron quantum optics is an emerging field that applies concepts and techniques from quantum optics to investigate the quantum properties and interference of individual charges in mesoscopic conductors [1–5]. Clean single-electron excitations can now be generated and emitted into a mesoscopic conductor without accompanying electron-hole pairs [6–9]. These dynamic excitations can be probed at the single-electron level in tomographic experiments [8–11], and they can be made to interfere [7, 12] and interact [13–15] at quantum point contacts that function as electronic beam splitters. In addition to fundamental investigations of charge pulses in mesoscopic conductors, electron quantum optics also holds promises for applications such as for current standards [16] and electronic flying qubits [17].

Up until now, experiments in electron quantum optics have been carried out with electrons and holes in metals or semiconductors [6–15]. However, the addition of superconductors would enable additional types of processes, for example, by allowing for Andreev reflections whereby an electron is converted coherently into a hole [18–21]. Such a conversion process of a particle into its anti-particle has no counterpart in quantum optics with photons and would thus be unique to electron quantum optics [22–25]. The inclusion of superconductivity to electron quantum optics seems promising, and it is motivated by several recent experiments where the edge states of a quantum Hall sample have been coupled to a superconductor [26–39]. Combined with techniques from electron quantum optics, one might explore the dynamic processes at the interfaces between normal metals and superconductors in the high-frequency regime [40–49]. Such a setup would enable quantum superpositions of states with different numbers of charges [50]. For example, Andreev processes would allow for the transformation of an electron into a superposition of an electron

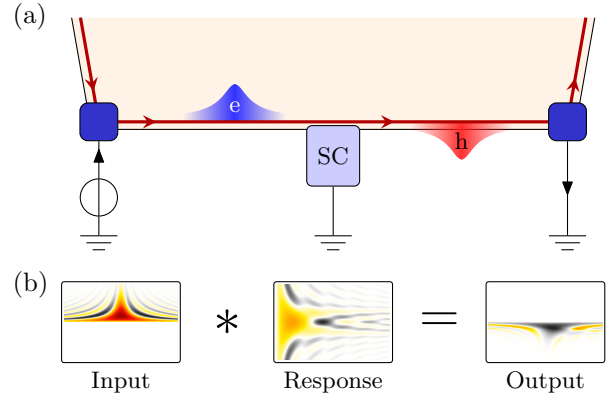


FIG. 1. Wigner representation of Andreev conversions. (a) Single-electron pulses are injected into a quantum Hall edge state and are scattered off the interface with a superconductor. The charge pulses can be either normal-reflected or Andreev converted at the interface, or they can be transmitted into the superconductor above the gap. (b) The response of the interface can be represented by a Wigner function describing the conversion of an input state to an output state, both represented by their Wigner function.

and a hole, which could find use for interferometric measurements and sensing [51].

Figure 1 illustrates the essential idea of our work. We consider voltage pulses that are applied to the edge states of a quantum Hall sample, so that single-electron excitations are emitted towards the interface with a superconductor. Here, they are either Andreev converted or normal-reflected back into the edge states, or they are transmitted into the superconductor above the gap. The wave functions of the incoming and the outgoing particles can be visualized by their Wigner functions in the mixed time and frequency representation [52–54], and they are related by the response function of the superconducting

interface as shown in the figure.

The rest of our article is organized as follows. In Sec. II, we employ a circuit model to describe the interface between a metal and a superconductor in one dimension. In Sec. III, we define the single-electron coherence and its Wigner representation. In Sec. IV, we analyse the response functions for singlet and triplet superconductors with and without an insulating barrier. In Sec. V, we consider lorentzian-shaped voltage pulses that generate clean single-particle excitations known as levitons. We then investigate how levitons are Andreev converted or normal-reflected on the superconductor. Finally, in Sec. VI, we present our conclusions together with an outlook on possible avenues for further developments. Some technical details of our calculations are deferred to App. A.

II. SUPERCONDUCTOR INTERFACE

A. Hamiltonian

In this section, we introduce a one-dimensional model of an interface between a normal-metal and a superconductor [55]. We consider conventional s -wave (or singlet) superconductors as well as unconventional p -wave (or triplet) superconductors that are connected to a normal-metal either directly (an NS junction) or with an insulator between them (an NIS junction). We then derive a circuit description of the superconductor, which we can solve for arbitrary incoming electronic wave functions.

We start by deriving a low-energy approximation of the BCS Hamiltonian for excitations that are generated close to the Fermi level. To this end, we consider the interacting part of the BCS Hamiltonian in one dimension,

$$\hat{H}_{\text{BCS}} = \int \frac{dk}{2\pi} \left(\Delta_{\sigma'\sigma}^* \hat{c}_{-k,\sigma} \hat{c}_{k,\sigma'} + \Delta_{\sigma\sigma'} \hat{c}_{k,\sigma}^\dagger \hat{c}_{-k,\sigma'}^\dagger \right), \quad (1)$$

with $\Delta_{\sigma\sigma'}$ being the pair potential and $\hat{c}_{k,\sigma}^\dagger$ and $\hat{c}_{k,\sigma}$ are the usual fermionic operators for electrons with spin σ . For simplicity, we will consider s -wave pairing. In this case, Δ is an even function of the momentum [56]. Furthermore, we will also make the simplifying assumption that Δ does not depend on the momentum.

In the following, a real-space representation of the Hamiltonian will be convenient since we consider the interface between a superconductor and a normal-metal. We focus on low-energy excitations near the Fermi level and can therefore treat left and right movers separately, since they form two independent chiral and linear branches as illustrated in Fig. 2. We then define the corresponding field operators as

$$\hat{\psi}_{\sigma,L}(x) = \int_0^\infty dk \hat{c}_{\sigma,k} e^{i(k-k_F)x} \quad (2)$$

and

$$\hat{\psi}_{\sigma,R}(x) = \int_{-\infty}^0 dk \hat{c}_{\sigma,k} e^{i(k+k_F)x}. \quad (3)$$

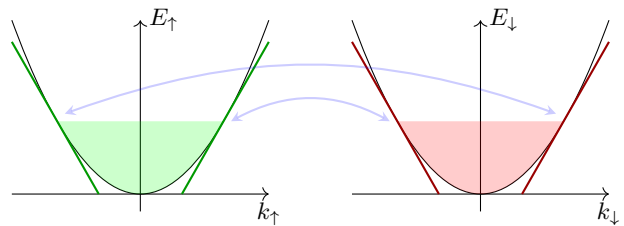


FIG. 2. Low-energy description. Close to the Fermi level, the dispersion relation can be linearized and left- and right-movers are coupled by the superconductor. For singlet superconductors, as shown, opposite spins are coupled.

The low-energy excitations have momenta that are close to the Fermi momentum, $k \simeq \pm k_F$. Thus, we can formally extend the integration limits to infinity and consider that we have two independent field operators that each fulfill the standard anti-commutation relations.

By expressing the BCS Hamiltonian in terms of these field operators, two types of terms appear. On the one hand, there are resonant terms that couple left and right movers, and which oscillate slowly in real-space. On the other hand, there are off-resonant terms that couple left movers to left movers and right movers to right movers. These terms have phases $e^{\pm 2ik_F x}$ that oscillate fast compared to the relevant excitation energies. Their contribution is thus negligible and they can be discarded below. With singlet pairing, we then arrive at the Hamiltonian

$$\hat{H}_{\text{singlet}} = \Delta^* \int dx [\hat{\psi}_{L,\downarrow}(x) \hat{\psi}_{R,\uparrow}(x) + \hat{\psi}_{R,\downarrow}(x) \hat{\psi}_{L,\uparrow}(x)] + \text{H.c.}, \quad (4)$$

with $\Delta \equiv \Delta_{\uparrow\downarrow}$. As illustrated in Fig. 2, this Hamiltonian couples $\hat{\psi}_{L,\downarrow}(x)$ to $\hat{\psi}_{R,\uparrow}(x)$ and $\hat{\psi}_{R,\downarrow}(x)$ to $\hat{\psi}_{L,\uparrow}(x)$ by the amplitude Δ .

A similar derivation can be carried out for a triplet superconductor. For pairings of fermions with the same spin, the Hamiltonian in momentum representation reads

$$\hat{H}_{\text{triplet}} = \int \frac{dk}{2\pi} \left(\Delta^* \hat{c}_{-k} \hat{c}_k + \Delta \hat{c}_k^\dagger \hat{c}_{-k}^\dagger \right), \quad (5)$$

where $\Delta \equiv \Delta_{\sigma\sigma}$ is now an odd function of the momentum [56]. In real-space, the Hamiltonian then becomes

$$\hat{H}_{\text{triplet}} = \Delta^* \int dx \hat{\psi}_L(x) \hat{\psi}_R(x) + \text{H.c.} \quad (6)$$

B. Circuit description

We first consider the scattering of electrons by a thin slice of a superconductor as in Fig. 3. Since the Hamiltonian is local, the superconductor can be described by stacking many of these small slices. Thus, we consider the scattering of incoming electrons by a superconductor of thickness dx . The Hamiltonian being quadratic, the

scattering process is linear. Furthermore, an incoming electron from the left will be scattered as an outgoing superposition of a left-moving hole and a right-moving electron.

We aim to describe the state in the normal-metal region far from the superconductor. Moreover, due to the linear dispersion, time and position are equivalent, and we may express the state of an electron as

$$|\varphi^{(e)}\rangle = v_F \int \varphi^{(e)}(v_F t) |v_F t\rangle dt, \quad (7)$$

where $\varphi^{(e)}(x) = \langle x|\varphi^{(e)}\rangle$ is the wave function of the electron, and we have used that $x = v_F t$. This time representation will turn out to be very convenient. First of all, we may work with a fixed position far from any interfaces and instead vary time. Second, from a practical point of view, measurements are typically carried out at fixed positions and the data is acquired as a function of time or frequency. With this in mind, we will express the bras and kets in the time representation mainly.

If an incoming electron scatters off the superconductor, two processes can occur. The first one is an Andreev conversion of the electron as a hole, which happens with an amplitude that is proportional to the thickness of the slice dx . Since we are considering a thin slice of superconductor, much smaller than the typical size of the wave packet, the response is expected to be constant over a wide range of frequencies. The state of the outgoing hole is then given by $\mathcal{C}|\varphi^{(e)}\rangle$, where \mathcal{C} is the anti-unitary operator that describes the conversion of an electron into a hole. In the time domain, this operator is given by complex conjugation as $(\mathcal{C}\varphi^{(e)})(t) = [\varphi^{(e)}(t)]^*$. It is, however, more convenient to describe the conversion of an electron into a hole in the frequency domain. If we define $\varphi^{(e)}(\omega)$ as the Fourier transform of $\varphi^{(e)}(t)$, we see that $(\mathcal{C}\varphi^{(e)})(\omega) = [\varphi^{(e)}(-\omega)]^*$. Thus, the operator \mathcal{C} transforms positive frequencies into negative ones and vice versa without changing the wave packet, which corresponds to the wideband assumption above.

The second process that can occur is normal transmission through the superconductor, in which the outgoing electron is delayed by the time dx/v_F . We can express both of these processes using the second quantization. Hence, we introduce the operators

$$\hat{\psi}_{L/R}^\dagger[\varphi] = v_F \int \varphi(t) \hat{\psi}_{L/R}^\dagger(t) dt \quad (8)$$

that create left or right-moving electrons in the wave function φ . We can represent the scattering process as a linear transformation between creation and annihilation operators described by the Bogoliubov transformation

$$\hat{\psi}_R^\dagger[\varphi^{(e)}] \rightarrow \hat{\psi}_R^\dagger[T_{dx/v_F}\varphi^{(e)}] + i\frac{dx\Delta}{\hbar v_F} \hat{\psi}_L[\mathcal{C}\varphi^{(e)}], \quad (9)$$

where T_{dt} is an operator that translates time by the duration dt .

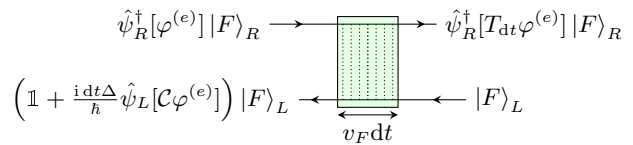


FIG. 3. Andreev conversion on a thin superconductor. An incoming electron can either be transmitted through the superconductor or be Andreev reflected as a hole. The transmitted electron is delayed by the time $dt = dx/v_F$, where dx is the width of the superconductor and v_F is the Fermi velocity.

Finally, one has to describe the ground state for the system composed by the slice of superconductor surrounded by the two normal metals. This case is actually pretty simple since if the three subsystems are at zero temperature and at the same chemical potential they are at equilibrium. As such, an easy ground state consists of two incoming Fermi sea at the chemical potential of the superconductor. The transformation in Eq. (9) should then be applied on this state. Hence, the processes in Fig. 3 can occur if a single electron arrives on the left side of the superconductor, so that either an electron is transmitted through the superconductor or a hole is Andreev reflected.

C. NS junction

We now focus on the scattering off an interface between a normal-metal and a superconductor. The central idea is to decompose the semi-infinite superconductor into thin slices as shown in Fig. 4. This approach is valid if we assume that the coupling Δ does not depend on the wave vector k nor on the position within the superconductor.

An incoming electron can be Andreev converted as a hole or it may propagate inside the superconductor. The latter case corresponds to the transmission of an electron from the metal into the superconductor, which can occur if the energy of the electron is above the gap. For this reason, the outgoing state is not a pure state, but rather a statistical mixture of a filled Fermi sea and a Fermi sea with a hole. The state of the outgoing hole reads

$$\sqrt{p} |\varphi_{\text{out}}^{(h)}\rangle = \mathcal{C}\mathcal{L}[|\varphi_{\text{in}}^{(e)}\rangle], \quad (10)$$

where p is the probability to have a conversion into a hole and \mathcal{L} is a linear operator that describes the response of the superconductor, which we wish to determine.

To describe the NS interface we use the discrete element model depicted in Fig. 4(b). Using the fact that the superconductor is semi-infinite and that the wave function should be smooth we find the following equation for the operator \mathcal{L} (for the full derivation, see App. A)

$$\frac{\Delta}{\hbar} |\varphi_{\text{in}}^{(e)}\rangle + 2\omega \mathcal{L}[|\varphi_{\text{in}}^{(e)}\rangle] + \frac{\Delta^*}{\hbar} \mathcal{L}^2[|\varphi_{\text{in}}^{(e)}\rangle] = 0. \quad (11)$$

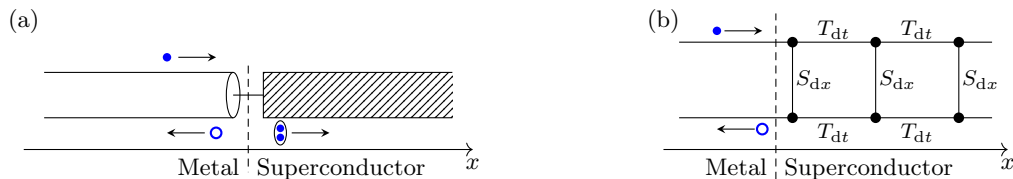


FIG. 4. Andreev conversion on a superconductor. (a) An incoming electron is reflected as a hole by the superconductor, where a Cooper pair is formed. (b) Inside the superconductor electrons can propagate ballistically, as described by the operator T_{dt} , or be Andreev reflected, as described by the operator S_{dx} . Here, a small time-step is denoted by dt , and $dx = v_F dt$.

Since \mathcal{L} is linear and invariant under time translations, we can express its action in the frequency domain as

$$\mathcal{L}[\psi](\omega) = \kappa(\omega)\psi(\omega) \quad (12)$$

and the equation for the response function $\kappa(\omega)$ becomes

$$\kappa^2(\omega) + 2\frac{\hbar\omega}{\Delta^*}\kappa(\omega) + \frac{\Delta}{\Delta^*} = 0. \quad (13)$$

Moreover, writing the pairing potential as $\Delta = e^{i\varphi}|\Delta|$ and imposing that the response function is bounded and causal we find the physical solution

$$\kappa(\omega) = e^{i\varphi}\Gamma(\omega), \quad (14)$$

where we have defined (with $x = \hbar\omega/|\Delta|$)

$$\Gamma(x) = \begin{cases} x + \sqrt{x^2 - 1}, & \text{if } x < -1 \\ x - i\sqrt{1 - x^2}, & \text{if } -1 \leq x \leq 1, \\ x - \sqrt{x^2 - 1}, & \text{if } x > 1 \end{cases} \quad (15)$$

or, equivalently in the complex plane,

$$\Gamma(z) = z - \sqrt{z + 1 + i0^+}\sqrt{z - 1 + i0^+}. \quad (16)$$

This particular solution has a single branch cut in the lower complex half-plane for $z \in [-1 - i0^+, 1 - i0^+]$, which ensures that the response is causal. Indeed, we can return to the time-domain by an inverse Fourier transform,

$$\Gamma(t) = \frac{1}{2\pi} \int_{-\infty}^{\infty} \Gamma(x) e^{-ixt|\Delta|/\hbar} dx. \quad (17)$$

For $t < 0$, we close the contour in the upper half plane and the integral vanishes since no branch cuts or poles are enclosed. For $t > 0$, we instead evaluate the integral along the branch cut in the lower half plane and find

$$\Gamma(t) = -i\Theta(t) \frac{J_1(|\Delta|t/\hbar)}{t}, \quad (18)$$

where $J_n(t)$ are the Bessel functions of the first kind and $\Theta(t)$ is a step function which ensures a causal response.

D. NIS junction

To describe the NIS junction we add an insulating layer that acts as a tunnel barrier between the normal-metal

and the superconductor. The barrier can be described by its transmission and reflection amplitudes, $t(\omega)$ and $r(\omega)$, which to a good approximation can be taken to be frequency-independent. The setup resembles a Fabry-Pérot interferometer with both the insulator and the superconductor acting as reflecting mirrors [57]. We can then sum up the amplitudes for all possible processes, and for a singlet superconductor we find

$$r_{ee}(\omega) = r \frac{1 - \Gamma^2(\omega)}{1 - |r|^2 \Gamma^2(\omega)}, \quad (19)$$

and

$$r_{eh}(\omega) = t^{*2} e^{i\varphi} \frac{\Gamma(\omega)}{1 - |r|^2 \Gamma^2(\omega)}, \quad (20)$$

where we have used that $\kappa(\omega)\kappa^*(-\omega) = -\Gamma^2(\omega)$ for a return trip inside the interferometer.

The case of a triplet superconductor is somewhat subtle because the outgoing fields from the interferometer are the same. In that case, an extra phase of π is acquired during the return trip within the interferometer and the reflection amplitudes then become

$$r_{ee}(\omega) = r \frac{1 + \Gamma^2(\omega)}{1 + |r|^2 \Gamma^2(\omega)}, \quad (21)$$

and

$$r_{eh}(\omega) = -t^{*2} e^{i\varphi} \frac{\Gamma(\omega)}{1 + |r|^2 \Gamma^2(\omega)}, \quad (22)$$

which have different signs compared to the singlet case.

III. WIGNER FUNCTION

A. First-order coherence

To describe the electronic excitations, we consider the first-order coherence function defined as [1, 57–62]

$$\mathcal{G}_{x,x}^{(e)}(t, t') = \langle \hat{\psi}^\dagger(x', t') \hat{\psi}(x, t) \rangle, \quad (23)$$

where the position x may also function as a channel and spin index. Typically, we consider a fixed position and omit this index. We also define the hole coherence as

$$\mathcal{G}_{x,x}^{(h)}(t, t') = \langle \hat{\psi}(x', t') \hat{\psi}^\dagger(x, t) \rangle. \quad (24)$$

Both of the first-order coherences obey the Hermitian symmetry $\mathcal{G}_{x,x'}^{(e/h)}(t,t') = [\mathcal{G}_{x',x}^{(e/h)}(t',t)]^*$. Also, because of the fermionic anticommutation relations, we have

$$\mathcal{G}_{x,x'}^{(e)}(t,t') + \mathcal{G}_{x',x}^{(h)}(t',t) = \delta[(x - v_F t) - (x' - v_F t')] . \quad (25)$$

In addition, one can define the excess coherence,

$$\Delta\mathcal{G}^{(e/h)} = \mathcal{G}^{(e/h)} - \mathcal{G}_{\mu,T}^{(e/h)}, \quad (26)$$

where the equilibrium contribution $\mathcal{G}_{\mu,T}^{(e/h)}$ from the Fermi sea at chemical potential μ and temperature T has been subtracted. We may then express the electric current as

$$i(t) = -ev_F \Delta\mathcal{G}^{(e)}(t,t), \quad (27)$$

which vanishes at equilibrium where $\mathcal{G}^{(e/h)} = \mathcal{G}_{\mu,T}^{(e/h)}$.

B. Wigner representation

The first-order coherences in Eqs. (23,24) provide information about the electronic state in the time-domain. To visualize this information, we here adopt the time-frequency Wigner representation defined as [52–54]

$$W(t,\omega) = v_F \int \mathcal{G}(t + \tau/2, t - \tau/2) e^{i\omega\tau} d\tau. \quad (28)$$

While the Wigner function is real, it is in general not positive, nor bounded from above by one. For electrons, values below zero or above one indicate non-classicality. We also introduce the excess Wigner function,

$$\Delta W = W - W_{\mu,T}, \quad (29)$$

where we again subtract the contribution from the Fermi sea. The current can then be written as

$$i(t) = -e \int \Delta W^{(e)}(t,\omega) \frac{d\omega}{2\pi}, \quad (30)$$

while the excess occupation number at energy $\hbar\omega$ reads

$$\Delta n(\omega) = \overline{\Delta W^{(e)}(t,\omega)}^t. \quad (31)$$

Here, the overline denotes an average over a period for periodic drives and an integral over time for non-periodic drives. The anticommutation relations imply that

$$W^{(e)}(t,\omega) + W^{(h)}(t,-\omega) = 1, \quad (32)$$

and

$$\Delta W^{(e)}(t,\omega) + \Delta W^{(h)}(t,-\omega) = 0. \quad (33)$$

Wigner representations are also useful to visualize the scattering process in itself. First of all, both linear and antilinear transformations acting on the wavefunctions can be represented by linear transformations on

the Wigner functions. Furthermore, the transformations that are invariant by time translations have a particularly simple form and can be associated with a Wigner function.

First of all, any antilinear transformation can be represented as the combination of a linear transformation and the electron-hole transformation given by the \mathcal{C} operator introduced earlier. The latter transforms electrons into holes and vice versa, corresponding to the transformation that maps $\Delta W^{(e)}$ to $\Delta W^{(h)}$ or, equivalently,

$$\Delta W(t,\omega) \mapsto -\Delta W(t,-\omega). \quad (34)$$

In addition, any time-invariant linear scattering process that transforms the operator $\hat{\psi}(t) \rightarrow \int \kappa(t-t') \hat{\psi}(t') dt'$, where κ is the response function, can be associated to the Wigner function of the response, defined as

$$W_\kappa(t,\omega) = \int \kappa(t + \tau/2) \kappa^*(t - \tau/2) e^{i\omega\tau} d\tau. \quad (35)$$

The Wigner function of the outgoing state is then given by the incoming one convolved with the response as [63]

$$W^{(\text{out})}(t,\omega) = \int W_\kappa(t-t',\omega) W^{(\text{in})}(t',\omega) dt. \quad (36)$$

As such, the Wigner function W_κ provides a convenient visualization of the response function. Its marginals contain information about the response in the time and in the frequency domain. The marginal in frequency yields the probability of a wave packet with a given frequency to be transmitted. Similarly, the marginal in time yields the modulus squared of the response, $|\kappa(t)|^2$. It is also possible to extract the time delay of a wave packet at a given frequency. If a wave packet is peaked around the frequency ω , with a width that is small compared to the variations of the Wigner function of the response, it will experience the time delay [63]

$$\tau(\omega) = \int t W_\kappa(t,\omega) dt = \text{Im}[\kappa'(\omega)/\kappa(\omega)]. \quad (37)$$

IV. RESPONSE FUNCTION

A. NS junction

We now investigate the response functions of the NS and NIS junctions. In general, we have four different responses, two for normal electron-electron and hole-hole processes, and two for electron-hole and hole-electron conversion processes. However, due to the electron-hole symmetry, we can focus on just two of them, for example, the normal electron-electron processes and the Andreev electron-hole conversion processes. We start with the NS junction, for which there are no normal reflections, and it suffices to consider the conversion processes only.

The response of the NS junction is given by Eqs. (14,15). Thus, an incoming electron with the wave

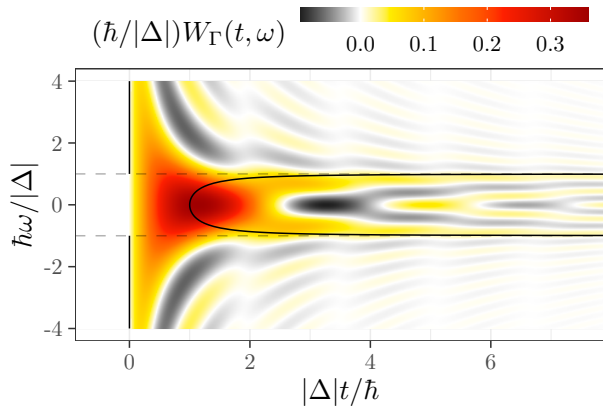


FIG. 5. Wigner representation of the response function of an NS junction. The gap is marked by the dashed line while the black line represents the delay time $\tau_{\text{NS}}(\omega)$.

function $\varphi^{(e)}(\omega)$ will be converted into a hole with the wave function $\varphi^{(h)}(\omega)$ according to the relation

$$\sqrt{p}[\varphi^{(h)}(-\omega)]^* = \Gamma(\omega)\varphi^{(e)}(\omega). \quad (38)$$

Here, the probability of conversion can be expressed as

$$p = \int_0^\infty |\Gamma(\omega)\varphi^{(e)}(\omega)|^2 d\omega, \quad (39)$$

which ensures that $\varphi^{(h)}$ is properly normalized. We can also revert Eq. (38) to the time-domain as

$$\sqrt{p}\varphi^{(h)}(t)^* = \int \Gamma(t-t')\varphi^{(e)}(t')dt', \quad (40)$$

showing how the incoming wave packet is modified.

To analyze the conversion probability at frequency ω , we notice that $\Gamma(\omega)$ in Eq. (15) takes the form $\Gamma(\omega) = e^{-i \arccos(\hbar\omega/|\Delta|)}$ for $|\hbar\omega| \leq |\Delta|$. Thus, for a wave packet with energies inside the gap the conversion probability is one. However, at higher energies, the probability of conversion decays. Indeed, there is a chance that an electron containing energies above the gap escapes into the superconductor. Conversely, a simple case is when the energies of the incoming wave packet are well inside the gap, such that $|\hbar\omega| \ll |\Delta|$. Since we have $\Gamma(\omega) \simeq -ie^{i\hbar\omega/|\Delta|}$ the outgoing wave packet is not deformed but only delayed by the time $\tau_{\text{NS}} = \hbar/|\Delta|$. More generally, we find the delay time at frequency ω

$$\tau_{\text{NS}}(\omega) = \frac{\hbar}{\sqrt{|\Delta|^2 - (\hbar\omega)^2}} \quad (41)$$

for energies inside the gap according to Eq. (37). Here we see that the delay time diverges as we approach the superconducting gap. By contrast, above the gap the delay time is zero and the scattering process is instantaneous.

These observations can be visualized by the Wigner function in Fig. 5. Clearly, the response is causal, as one

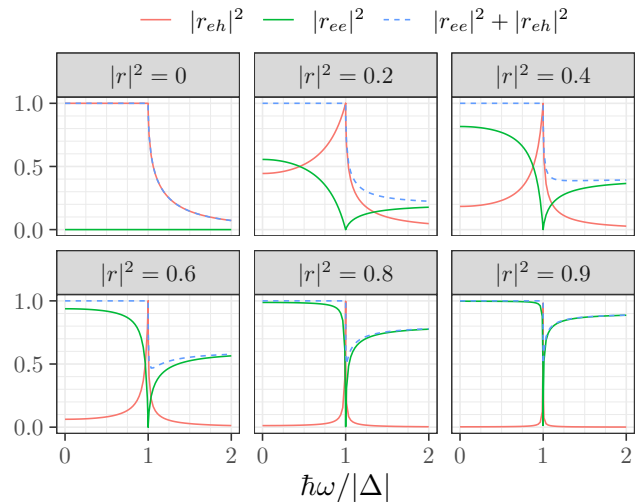


FIG. 6. Probabilities for Andreev conversions and normal-reflections on an NIS junction with a singlet superconductor.

would expect since $W(t, \omega) = 0$ for $t < 0$. We also indicate the delay time given by Eq. (41) (black line), which is related to the Wigner function according to Eq. (37). In the Wigner function of the response, we see a difference in the oscillations above and below the gap. In particular, above the gap the positive and negative parts tend to balance out. Indeed, because the Wigner function is causal, and the time delay above the gap is zero, we have

$$\int_0^\infty W(t, \omega)t dt = 0, \quad (42)$$

which causes the positive and negative parts to cancel out. By contrast, inside the gap the time delay is finite and it even diverges close to the gap, which explains the different oscillatory behaviors above and below the gap.

The interpretation of $\tau_{\text{NS}}(\omega)$ as a delay time is only valid for wave functions that are centered around ω with a small bandwidth compared to the frequencies over which the time delay changes. Conversely, the duration of the wave packet must be large compared to the oscillations in the Wigner function at this frequency. Hence, for frequencies close to the gap edge in Fig. 5, where the delay time diverges, the wave functions must be very wide in order not to change shape due to the scattering.

B. NIS junction – singlet superconductor

We now consider the NIS junction, focusing first on singlet superconductors. For the NIS junction, incoming electrons can be converted into holes with the amplitude $r_{eh}(\omega)$ according to Eq. (20). However, due to the insulating barrier, they may also be reflected as electrons with amplitude $r_{ee}(\omega)$ according to Eq. (19). Thus, we have to consider both processes in our analysis.

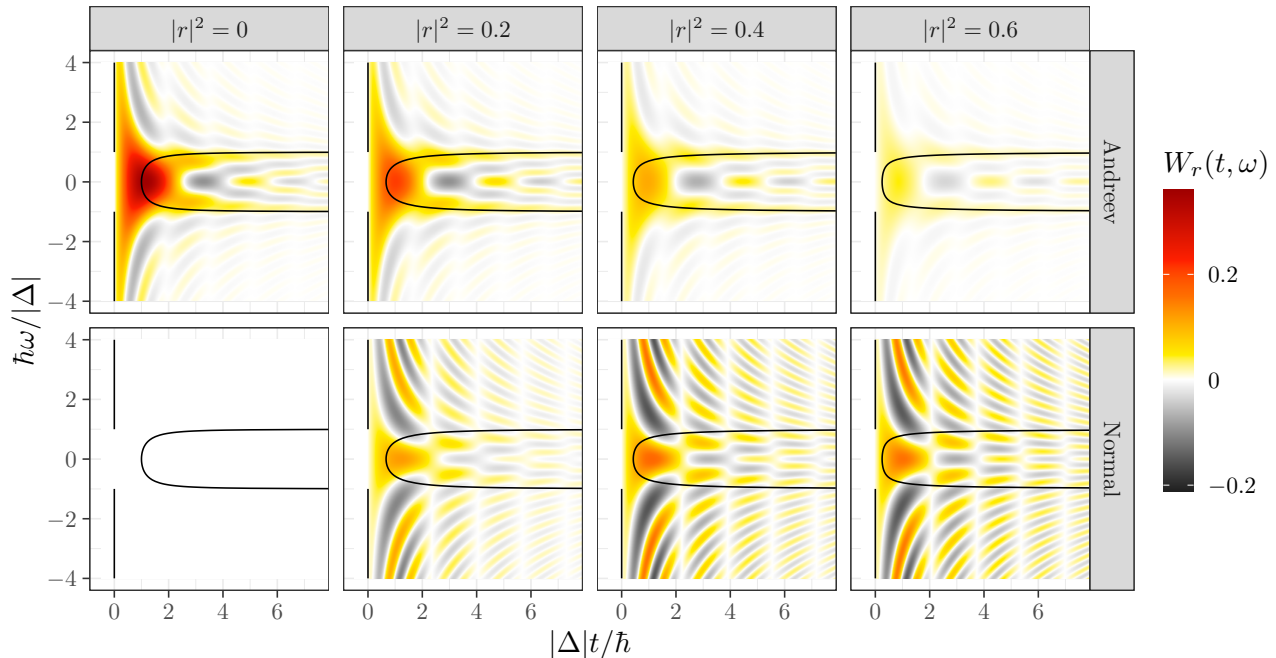


FIG. 7. Wigner representation of the response function for an NIS junction with a singlet superconductor. The top row shows the Andreev conversions and the bottom row the normal-reflections. The black line indicates the delay time $\tau_S(\omega)$.

We first analyze the amplitudes at a given frequency. For energies within the gap, electrons are never transmitted into the superconductor and we have $|r_{ee}(\omega)|^2 + |r_{eh}(\omega)|^2 = 1$. Above the gap, electrons can be transmitted into the superconductor and the sum is smaller than one. At very high energies, the amplitude for electron-hole conversion vanishes and electrons are either reflected back into the edge channel with probability $|r|^2$ or they are transmitted into the superconductor with probability $1 - |r|^2$. As such, we can interpret $|r|^2$ as the probability of normal reflections at very high energies.

Figure 6 shows the probabilities of normal reflections and Andreev conversions for different reflection probabilities of the insulating barrier. The conversion probability has a local minimum at zero energy. Furthermore, there is a resonance peak at the gap edge where the probability for electron-hole conversion is one. Moreover, when the reflection probability of the insulating barrier approaches one a discontinuity develops around the gap for the sum $|r_{ee}|^2 + |r_{eh}|^2$. This surprising feature implies that, if a wavepacket is emitted slightly above the gap, its probability of escaping into the superconductor can increase as $|r|^2$ increases. At low energies, we can expand the amplitudes to first order in $\hbar\omega/|\Delta|$ as

$$r_{ee}(\omega) \simeq \frac{2r}{1+|r|^2} \left(1 + i \frac{\hbar\omega}{|\Delta|} \frac{1-|r|^2}{1+|r|^2} \right), \quad (43)$$

and

$$r_{eh}(\omega) \simeq -i \frac{t^{*2} e^{i\varphi}}{1+|r|^2} \left(1 + i \frac{\hbar\omega}{|\Delta|} \frac{1-|r|^2}{1+|r|^2} \right). \quad (44)$$

Thus, at zero energy the normal reflection probability is $4|r|^2/(1+|r|^2)^2$, while the Andreev conversion probability reads $(1-|r|^2)^2/(1+|r|^2)^2$. The interference due to the barrier leads to an enhancement of the normal reflections while it reduces the Andreev conversions.

For both processes, the time delay at low energies reads

$$\tau_S(\omega) \simeq \frac{\hbar}{|\Delta|} \frac{1-|r|^2}{1+|r|^2}. \quad (45)$$

Surprisingly, the time delay decreases with increasing reflection probability and it vanishes as the reflection probability approaches one. It must be noted that this happens only when the conversion processes have some “losses”, either in the form of trivial reflection or through leakage in the superconductor, when the electron is emitted above the gap. The fact that the conversion process becomes faster than the typical time, \hbar/Δ , or even instantaneous when the electron is emitted above the gap, may seem to violate causality. However, in lossy system, this is a relatively common occurrence, and it can be seen as a destructive interference process, that does not violate causality [64–66].

At low energies, we may also express the outgoing current in terms of the incoming one as

$$i_{\text{out}}(t) \simeq \left(\frac{8|r|^2}{(1+|r|^2)^2} - 1 \right) i_{\text{in}}(t). \quad (46)$$

From this expression we see that the current vanishes for $|r|^2 = 3 - \sqrt{8} \simeq 0.17$, implying that the number of reflected electrons and holes exactly cancel out in that

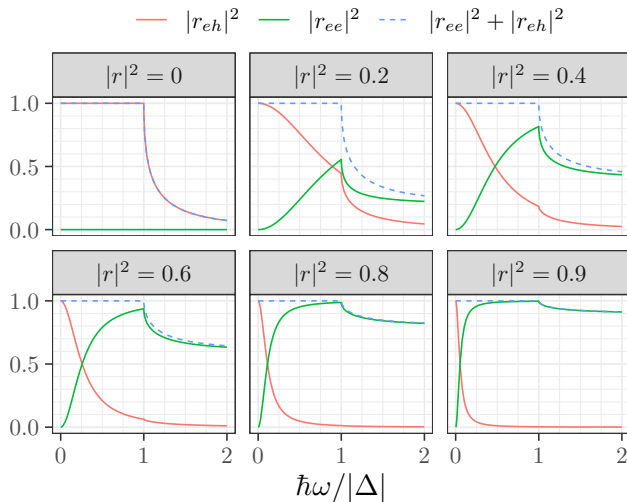


FIG. 8. Probabilities for Andreev conversions and normal reflections on an NIS junction with a triplet superconductor.

case. Interestingly, this cancellation occurs well below $|r|^2 = 0.5$ because of the reduction of the electron-hole conversion processes due to the barrier.

Figure 7 shows the Wigner representation of the conversion processes and the reflection processes for different probabilities of reflections on the barrier. Increasing the reflection probability, the conversion processes are reduced and the reflection of electrons on the interface becomes increasingly dominant. In addition, we notice a resonance in the conversion process at energies close to the gap. In the figure, we also show the delay time for energies inside gap, which can be written as

$$\tau_S(\omega) = \tau_{NS}(\omega) \left(1 - 2|r|^2 \frac{(1 + |r|^2) - 2(\hbar\omega/|\Delta|)^2}{(1 + |r|^2)^2 - 4|r|^2(\hbar\omega/|\Delta|)^2} \right), \quad (47)$$

where $\tau_{NS}(\omega)$ is the delay time for the NS junction. From this expression we see that the delay is decreased compared to the NS junction for small energies, $|\hbar\omega/|\Delta| < \sqrt{(1 + |r|^2)/2}$, while it is increased for larger energies.

C. NIS junction – triplet superconductor

We can carry out a similar analysis for the NIS junction with a triplet superconductor. Similarly to the singlet superconductor, at energies well above the superconducting gap incoming electrons are either normal reflected with probability $|r|^2$ or they are transmitted into the superconductor with probability $1 - |r|^2$; moreover, there is no Andreev conversion. At lower energies, the triplet and the singlet cases are different because of the different signs between Eqs. (19,20) for a singlet superconductor and Eqs. (21,22) for a triplet superconductor.

In Fig. 8 we show the normal reflection and Andreev conversion probabilities for the triplet superconductor,

which can be compared with the results for the singlet superconductor in Fig. 6. First, unlike the singlet case, the sum $|r_{ee}|^2 + |r_{eh}|^2$ is smoother as $|r|^2$ approaches one. Hence, transmissions into the superconductor are always reduced as $|r|^2$ increases. We also notice that there is always perfect conversion at zero energy. The conversion probability then goes down with increasing energy and with increasing reflection amplitude of the barrier. In particular, with a large reflection amplitude the conversion process develops a narrow peak around zero energy. At low energies, we can expand the amplitudes to first order in $\hbar\omega/|\Delta|$ as

$$r_{ee}(\omega) \simeq -2i \frac{r}{1 - |r|^2} \frac{\hbar\omega}{|\Delta|}, \quad (48)$$

and

$$r_{eh}(\omega) \simeq i \frac{t^{*2}}{|t|^2} e^{i\varphi} \left(1 + i \frac{\hbar\omega}{|\Delta|} \frac{1 + |r|^2}{1 - |r|^2} \right). \quad (49)$$

For normal reflections we then have $|r_{ee}(\omega)|^2 \simeq 4|r|^2(\hbar\omega/|\Delta|)^2$, which vanishes quadratically with the energy. For the conversion processes we find at low energies

$$\tau_T(\omega) \simeq \frac{\hbar}{|\Delta|} \frac{1 + |r|^2}{1 - |r|^2}, \quad (50)$$

which is larger than $\hbar/|\Delta|$ and diverges as the reflection probability approaches one. For the expansions above to be valid the energies must be such that $|\hbar\omega| \ll |\Delta|, (1 - |r|^2)|\Delta/r|$. Thus, the frequency bandwidth for which these expansions hold decreases as the reflection probability goes to one. In turn, the delay time stays small compared to the typical width of an incoming wave packet.

Figure 9 shows the Wigner representations of the two processes for different reflection probabilities of the barrier. As the reflection probability increases, the Andreev conversion processes are reduced and the normal reflections become more pronounced. Still, the behavior is different from the singlet case. For the triplet case, we observe a resonance peak for the conversion processes at zero energy, while in the singlet case the resonance occurs at the gap edge. Moreover, the conversion processes for the singlet case are suppressed at low energies.

Also, for the triplet case we can express the delay time for energies inside the superconducting gap as

$$\tau_T(\omega) = \tau_{NS}(\omega) \left(1 + 2|r|^2 \frac{(1 - |r|^2) - 2(\hbar\omega/|\Delta|)^2}{(1 - |r|^2)^2 + 4|r|^2(\hbar\omega/|\Delta|)^2} \right), \quad (51)$$

where $\tau_{NS}(\omega)$ is the delay time for the NS junction. This expression is also different from the singlet case. At low energies, $|\hbar\omega/|\Delta| \leq \sqrt{(1 - |r|^2)/2}$, the time delay is longer than for the NS junction; otherwise, it is shorter.

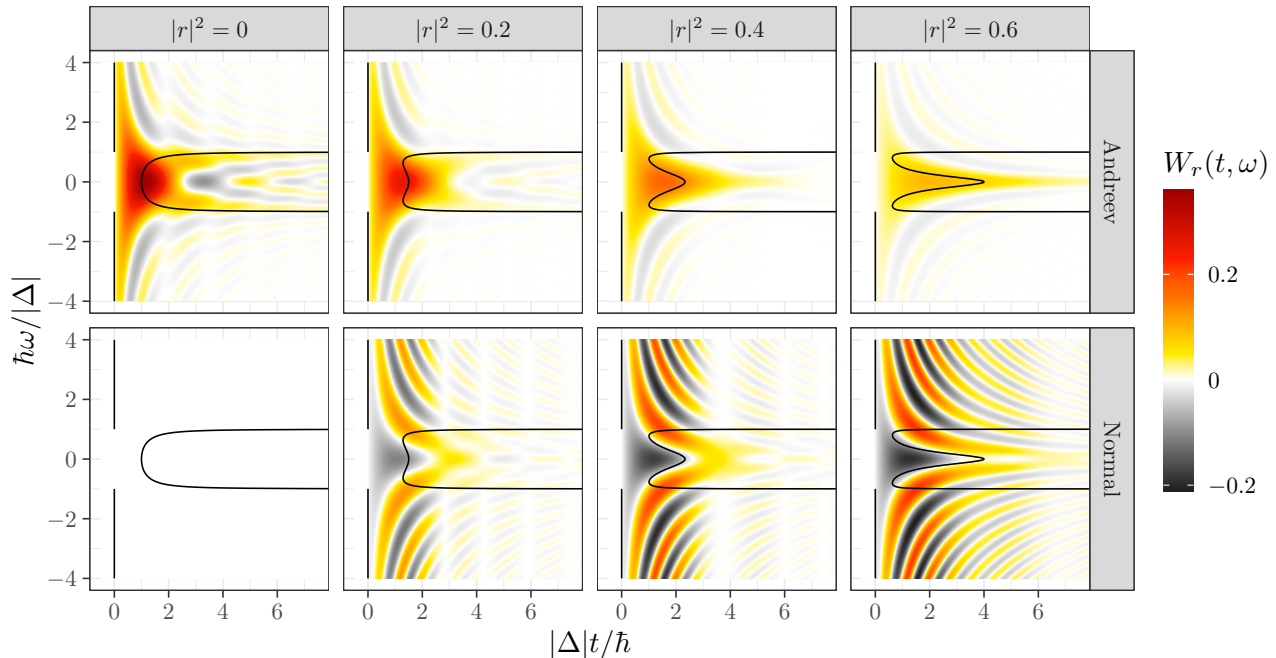


FIG. 9. Wigner representation of the response function for an NIS junction with a triplet superconductor. The top row shows the Andreev conversions, while the bottom row shows the normal-reflections. The black line indicates the delay time $\tau_T(\omega)$.

V. ANDREEV CONVERSION OF A LEVITON

A. Levitons

We can now consider the reflection and conversion of specific charge excitations. In particular, we are interested in periodic voltage pulses that excite an average charge of exactly one electron per period of the drive [67–72]. If the pulses are well-separated and lorentzian-shaped, they generate clean single-electron excitations known as levitons without exciting any additional electron-hole pairs in the Fermi sea [7, 8]. The injected wave function reads

$$\psi(t) = \sqrt{\frac{\tau_0}{v_F \pi}} \frac{1}{t - i\tau_0}, \quad (52)$$

whose modulus square is a lorentzian of width τ_0 . At zero temperature, we have $\Delta\mathcal{G}^{(e)}(t, t') = \psi^*(t')\psi(t)$ and the excess coherence of a leviton becomes

$$\Delta\mathcal{G}^{(e)}(t, t') = \frac{\tau_0}{v_F \pi} \frac{1}{(t - i\tau_0)(t' + i\tau_0)}. \quad (53)$$

Inserting this expression into Eq. (28) and evaluating the integral using complex-contour integration we find

$$\Delta W^{(e)}(t, \omega) = 8\omega\tau_0 \text{sinc}(2\omega t) e^{-2\omega\tau_0} \Theta(\omega), \quad (54)$$

which is the Wigner representation of a leviton. Moreover, the current is a lorentzian of width τ_0 ,

$$i(t) = -\frac{e\tau_0}{\pi(t^2 + \tau_0^2)}. \quad (55)$$

We also find that the excess occupation number is

$$\Delta n(\omega) = 4\pi\tau_0 e^{-2\omega\tau_0} \Theta(\omega), \quad (56)$$

showing that these excitations have an exponentially decaying distribution of energies. In Fig. 10, we show the Wigner representation of a leviton. In the following, it will be important to compare the width of the wave function with the superconducting gap since their ratio will determine to what extent the wave packet is inside the gap, or if it also contains energies above the gap.

B. NS junction

For the NS junction, the only possible process is the Andreev conversion. In Fig. 10, we show the electronic Wigner representation of an incoming leviton pulse and the hole Wigner representation of the outgoing holes for an NS junction. We consider different widths of the charge pulses compared to the gap of the superconductor. For the outgoing holes, we use the hole representation $W^{(h)}(t, \omega) = 1 - W^{(e)}(t, -\omega)$, which makes it easier to compare the Wigner functions for the incoming and the outgoing particles. For the outgoing particles, we also show the delay time $\tau_{\text{NS}}(\omega)$ with a green line.

The converted holes change shape depending on the width of the incoming leviton. If the incoming leviton is well within the gap, the converted hole is an anti-leviton that is delayed by the time $\hbar/|\Delta|$. That situation corresponds to the right-most panel in Fig. 10. We also see that the delay time $\tau_{\text{NS}}(\omega)$ is approximately equal to

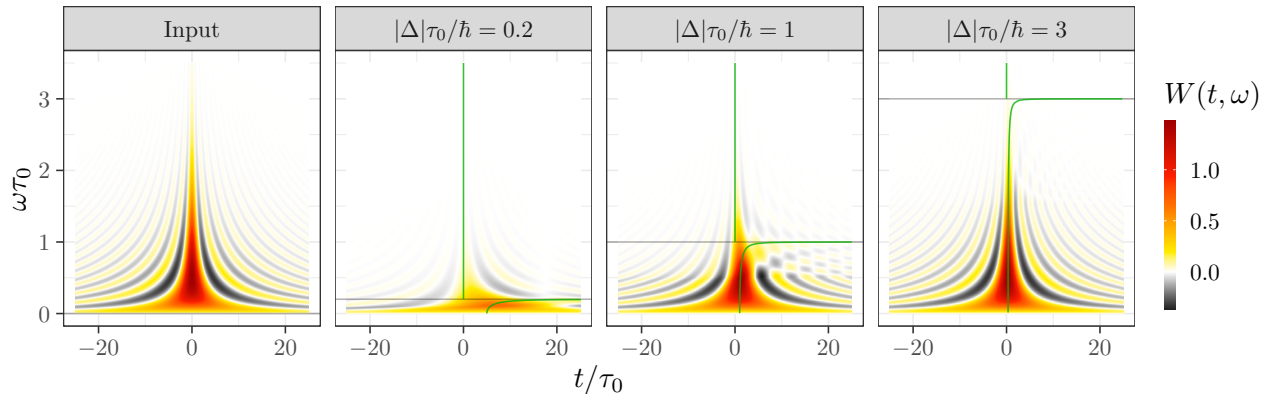


FIG. 10. Andreev reflection of a leviton on an NS junction. The left panel shows the electronic Wigner function $W^{(e)}(t, \omega)$ of an incoming leviton of width τ_0 . The other panels show the hole Wigner function $W^{(h)}(t, \omega) = 1 - W^{(e)}(t, -\omega)$ of an Andreev converted leviton of different widths. The gray lines indicate the gap and the green lines show the delay time $\tau_{NS}(\omega)$.

$\hbar/|\Delta|$ over the full frequency range of the leviton. Furthermore, the conversion process happens with a probability close to one. On the other hand, as the width of the leviton is decreased, the conversion happens with a probability that is smaller than one, since parts of the leviton may be transmitted into the superconductor. In that case, the reflected particle is no longer an anti-leviton as seen in the two central panels. If the frequencies of the incoming leviton become comparable to the gap, different frequency components experience different delays, which changes the shape of the reflected particles. We also notice the consequence of the divergence of the time delay around the gap. In the third panel of Fig. 10 the wave function is strongly deformed around these frequencies. By contrast, at energies well inside the gap the wave function is hardly changed, besides a time delay, since the Wigner function of the leviton oscillates slowly. In the second panel of Fig. 10, the probability for transmission into the superconductor is large. In this case, the leviton duration is extremely short compared to all the relevant scales of the problem. As such, the leviton becomes a wideband probe as the Wigner function of the reflected particle resembles the Wigner function of the response of the superconductor.

C. NIS junction

For the NIS junction, we have to consider both the Andreev conversions and the normal reflections. For that reason, both the time delay and the probability of reflections at a given frequency play a role, even within the gap. Inside the gap, the number of excitations (electrons and holes) is conserved and the conversion and reflection processes are complementary: If the probability of one of the processes decreases, it increases for the other.

In Fig. 11, we show the results for a normal-reflected and an Andreev converted leviton, both for singlet and triplet superconductors. To simplify the comparison

of the Andreev conversions and the normal-reflections, we show the Wigner function of the conversion processes as the Wigner representation of the hole coherence, $W^{(h)}(t, \omega) = 1 - W^{(e)}(t, -\omega)$. On the other hand, the Wigner function of the reflections is given by the electron coherence, $\Delta W^{(e)}(t, \omega)$. In this way, we can directly compare the converted and the reflected wave packets.

We first observe that the normal processes are favored over the Andreev processes as the reflection probability of the insulating barrier is increased, both for singlet and triplet superconductors. Still, comparing the singlet and triplet superconductors for a given reflection coefficient of the barrier, the singlet superconductor tends to favor the normal processes over the Andreev processes more than the triplet superconductor. We also see an attenuation of the Wigner functions at energies above the gap for the Andreev processes, which corresponds to transmission of excitations into the superconductor. By contrast, the normal processes do not exhibit this feature, which is consistent with the fact that they are simply given by reflections on the insulating barrier.

Altogether, the Wigner function visualizes the full frequency dependence of the two processes and it allows for an accurate comparison between singlet and triplet superconductors. For singlet superconductors, we see a long positive tail around the gap for the Andreev processes, corresponding to the resonance of the Andreev conversion at gap edge. As the barrier reflection increases, we observe that the tail becomes better defined and it grows longer, corresponding to a sharper energy filtering. Conversely, for the normal processes we see that the Wigner function oscillates quickly between positive and negative values around the gap edge, such that those frequencies are filtered out. Indeed, in the triplet case there is no such resonance around the gap. However, we observe that the low-frequency content of the Andreev conversions remains important even at high values of the barrier reflection because of the resonance at zero energy. Furthermore, we see that the center of the wave

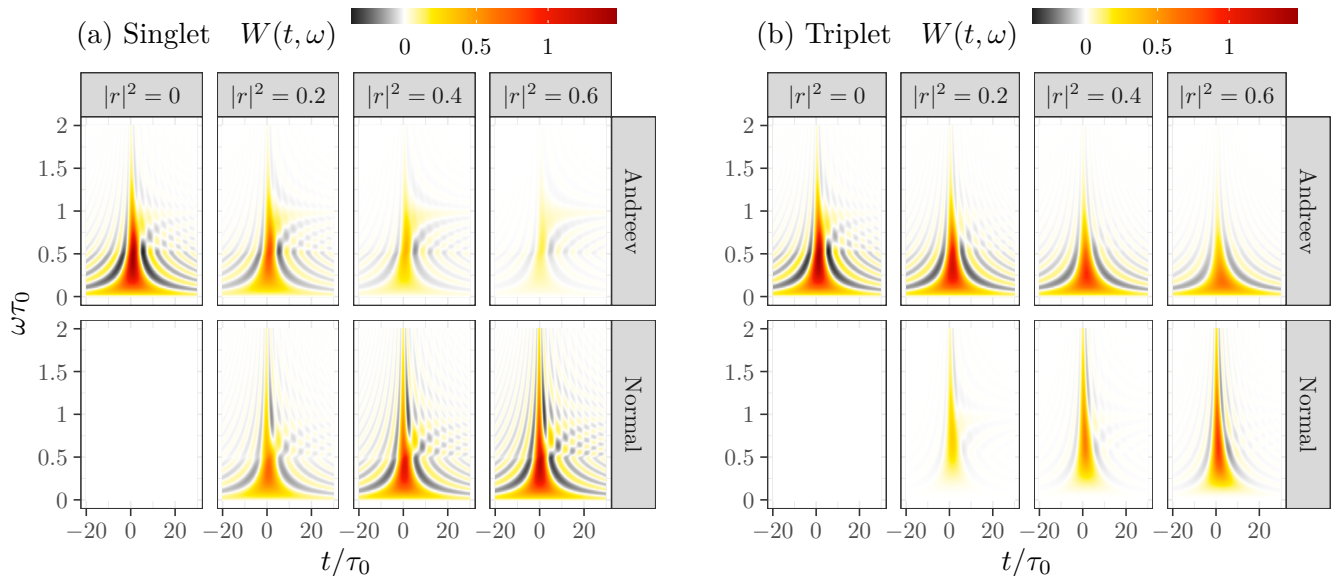


FIG. 11. Wigner functions for Andreev conversions and normal-reflections of a leviton. The Andreev conversions (top row) are represented by the hole Wigner function $W^{(h)}(t, \omega)$, while the normal reflections (bottom row) are represented by the electronic Wigner function $W^{(e)}(t, \omega)$. The two panels correspond to singlet (a) and triplet (b) superconductors. In each panel, we show results for different reflection probabilities of the insulating barrier. The width of the incoming leviton is fixed to $\tau_0 = \hbar/|\Delta|$.

packet at low energies is delayed as the barrier reflection increases. Conversely, the normal processes do not have any low-frequency components.

VI. CONCLUSIONS

We have employed a Wigner function representation to describe the scattering of single-electron charge pulses on the interface between a normal-metal and a superconductor. In particular, we have shown that Wigner functions provide an efficient way of visualizing both the response of the superconducting interface and the wave function of the outgoing particles thanks to the mixed time-and-frequency representation. From the Wigner functions several other quantities of interest can be extracted such as the time-dependent current, the probability for a charge at a particular frequency to be Andreev converted or normal-reflected at the interface, as well as the time delay associated with these processes.

We have considered junctions with and without an insulating barrier between the metal and the superconductor, which can have either singlet or triplet pairing. Without a barrier, there are no normal reflections at the interface and incoming charges are either Andreev converted or transmitted into the superconductor above the gap. With the insulating barrier at the interface, more processes become possible as incoming charges may also be normal-reflected at the interface. The Wigner function representation allows us to visualize how an incoming wave packet is deformed by the scattering off the

interface with the superconductor. Specifically, we have shown how the type of superconductor, being singlet or triplet, affects the response of the junction, for example by changing the probabilities of normal reflections at a given frequency and the associated time delay. These effects can be clearly seen in the Wigner function of Andreev converted and normal-reflected charge pulses.

Our work shows that techniques from electron quantum optics can be useful to explore the interface between superconductors and quantum Hall edge states. For example, by using time-dependent voltages one may obtain information beyond what is available from measurements with constant biases only [43, 46]. Beyond exploring the physics of such interfaces, superconductivity may enable new applications in electron quantum optics such as the conversion of electrons into holes [20], which is a process without any counterpart in conventional quantum optics with photons. Superconductors may also function as sources of spin entanglement by splitting the Cooper pairs in a superconductor into separated normal-state regions [73–76]. Furthermore, in terms of metrological applications of electron quantum optics, superconductivity may offer new possibilities, for instance, for the interferometric sensing of tiny magnetic fields.

VII. ACKNOWLEDGEMENTS

We thank M. V. Moskalets for useful discussions and acknowledge support from InstituteQ, Research Council of Finland through Finnish Centre of Excellence in

Quantum Technology (project No. 352925), the Spanish CM ‘‘Talento Program’’ project No. 2019-T1/IND-14088 and No. 2023-5A/IND-28927, the Agencia Estatal de Investigación project No. PID2020-117992GA-I00 and No. CNS2022-135950 and through the ‘‘María de Maeztu’’ Programme for Units of Excellence in R&D (CEX2023-001316-M).

Appendix A: Derivation of response function

To derive the response function of the NS junction, we consider a linear operator \mathcal{L}_x that transforms the incoming wave function at position x into the outgoing one as

$$|\varphi_{\text{out}}^{(h)}(x)\rangle = \mathcal{C}\mathcal{L}_x |\varphi_{\text{in}}^{(e)}(x)\rangle, \quad (\text{A1})$$

where \mathcal{C} is an anti-unitary operator that describes the conversion of an electron into a hole. In addition, the wave functions at x and $x + dx$ are related as

$$\begin{aligned} \mathcal{C} |\varphi_{\text{out}}^{(h)}(x)\rangle = & -S_{eh}^* |\varphi_{\text{in}}^{(e)}(x)\rangle \\ & + S_{ee}^* T_{dx/v_F} \mathcal{C} |\varphi_{\text{out}}^{(h)}(x + dx)\rangle, \end{aligned} \quad (\text{A2})$$

which follows from Fig. 4. The operator $T_{\delta t}$ translates time by δt , while S_{eh} describes Andreev reflections, and S_{ee} accounts for transmissions into the superconductor.

Since the junction is situated at $x = 0$, and the superconductor is considered to be semi-infinite, we have

$\mathcal{L}_x = \mathcal{L}$ inside the superconductor. We then find

$$\begin{aligned} \mathcal{L} |\varphi_{\text{in}}^{(e)}(x)\rangle = & -S_{eh}^* |\varphi_{\text{in}}^{(e)}(x)\rangle \\ & + S_{ee}^* T_{dx/v_F} \mathcal{L} |\varphi_{\text{in}}^{(e)}(x + dx)\rangle, \end{aligned} \quad (\text{A3})$$

having used Eq. (A1) to write

$$\mathcal{C} |\varphi_{\text{out}}^{(h)}(x)\rangle = \mathcal{L} |\varphi_{\text{in}}^{(e)}(x)\rangle. \quad (\text{A4})$$

In addition, we can write the incoming state as

$$\begin{aligned} |\varphi_{\text{in}}^{(e)}(x + dx)\rangle = & S_{ee} T_{dx/v_F} |\varphi_{\text{in}}^{(e)}(x)\rangle \\ & + S_{eh} \mathcal{L} |\varphi_{\text{in}}^{(e)}(x + dx)\rangle. \end{aligned} \quad (\text{A5})$$

We can then insert Eq. (A5) into Eq. (A3) to obtain

$$\begin{aligned} \mathcal{L} |\varphi_{\text{in}}^{(e)}(x)\rangle = & -S_{eh}^* |\varphi_{\text{in}}^{(e)}(x)\rangle \\ & + |S_{ee}|^2 T_{2dx/v_F} \mathcal{L} |\varphi_{\text{in}}^{(e)}(x)\rangle \\ & + S_{ee}^* S_{eh} T_{dx/v_F} \mathcal{L}^2 |\varphi_{\text{in}}^{(e)}(x + dx)\rangle, \end{aligned} \quad (\text{A6})$$

having used that \mathcal{L} commutes with $T_{\delta t}$.

Now, to lowest order in dx , we have $S_{eh} \simeq i\Delta dx/\hbar v_F$ and $S_{ee} \simeq 1$. In the frequency domain we also have $T_{dx/v_F} \simeq 1 - i\omega dx/v_F$. Assuming that $|\varphi_{\text{in}}^{(e)}(x)\rangle$ varies smoothly, such that $|\varphi_{\text{in}}^{(e)}(x + dx)\rangle \simeq |\varphi_{\text{in}}^{(e)}(x)\rangle + \partial_x |\varphi_{\text{in}}^{(e)}(x)\rangle dx$, we can rewrite Eq. (A6) as

$$\frac{\Delta^*}{\hbar} |\varphi^{(e)}\rangle + 2\omega \mathcal{L} |\varphi^{(e)}\rangle + \frac{\Delta}{\hbar} \mathcal{L}^2 |\varphi^{(e)}\rangle = 0, \quad (\text{A7})$$

where we have kept only terms to lowest order in dx . This expression is equivalent to Eq. (11) of the main text.

-
- [1] E. Bocquillon, V. Freulon, F. D. Parmentier, J.-M. Berroir, B. Plaças, C. Wahl, J. Rech, T. Jonckheere, T. Martin, C. Grenier, D. Ferraro, P. Degiovanni, and G. Fève, Electron quantum optics in ballistic chiral conductors, *Ann. Phys.* **526**, 1 (2014).
- [2] J. Splettstoesser and R. J. Haug, Single-electron control in solid state devices, *Phys. Status Solidi B* **254**, 1770217 (2017).
- [3] B. Roussel, C. Cabart, G. Fève, E. Thibierge, and P. Degiovanni, Electron quantum optics as quantum signal processing, *Phys. Status Solidi B* **254**, 1600621 (2017).
- [4] C. Bäuerle, D. C. Glattli, T. Meunier, F. Portier, P. Roche, P. Roulleau, S. Takada, and X. Waintal, Coherent control of single electrons: a review of current progress, *Rep. Prog. Phys.* **81**, 056503 (2018).
- [5] H. Edlbauer, J. Wang, T. Crozes, P. Perrier, S. Ouacel, C. Geffroy, G. Georgiou, E. Chatzikyriakou, A. Lacerda-Santos, X. Waintal, D. C. Glattli, P. Roulleau, J. Nath, M. Kataoka, J. Splettstoesser, M. Acciai, M. C. da Silva Figueira, K. Öztas, A. Trelakis, T. Grange, O. M. Yevtushenko, S. Birner, and C. Bäuerle, Semiconductor-based electron flying qubits: review on recent progress accelerated by numerical modelling, *EPJ Quantum Technol.* **9**, 21 (2022).
- [6] G. Fève, A. Mahe, J.-M. Berroir, T. Kontos, B. Plaças, D. Glattli, A. Cavanna, B. Etienne, and Y. Jin, An on-demand coherent single-electron source, *Science* **316**, 1169 (2007).
- [7] J. Dubois, T. Jullien, F. Portier, P. Roche, A. Cavanna, Y. Jin, W. Wegscheider, P. Roulleau, and D. Glattli, Minimal-excitation states for electron quantum optics using levitons, *Nature* **502**, 659 (2013).
- [8] T. Jullien, P. Roulleau, B. Roche, A. Cavanna, Y. Jin, and D. Glattli, Quantum tomography of an electron, *Nature* **514**, 603 (2014).
- [9] A. Assouline, L. Pugliese, H. Chakraborti, S. Lee, L. Bernabeu, M. Jo, K. Watanabe, T. Taniguchi, D. C. Glattli, N. Kumada, H.-S. Sim, F. D. Parmentier, and P. Roulleau, Emission and coherent control of Levitons in graphene, *Science* **382**, 1260 (2023).
- [10] R. Bisognin, A. Marguerite, B. Roussel, M. Kumar, C. Cabart, C. Chapelaine, A. Mohammad-Djafari, J.-M. Berroir, E. Bocquillon, B. Plaças, A. Cavanna, U. Gennser, Y. Jin, P. Degiovanni, and G. Fève, Quan-

- tum tomography of electrical currents, *Nat. Commun.* **10**, 3379 (2019).
- [11] J. Fletcher, N. Johnson, E. Locane, P. See, J. Griffiths, I. Farrer, D. Ritchie, P. Brouwer, V. Kashcheyevs, and M. Kataoka, Continuous-variable tomography of solitary electrons, *Nat. Commun.* **10**, 5298 (2019).
- [12] E. Bocquillon, V. Freulon, J.-M. Berroir, P. Degiovanni, B. Plaçais, A. Cavanna, Y. Jin, and G. Fève, Coherence and indistinguishability of single electrons emitted by independent sources, *Science* **339**, 1054 (2013).
- [13] N. Ubbelohde, L. Freise, E. Pavlovskaya, P. G. Silvestrov, P. Recher, M. Kokainis, G. Barinova, F. Hohls, T. Weimann, K. Pierz, and V. Kashcheyevs, Two electrons interacting at a mesoscopic beam splitter, *Nat. Nanotech.* **18**, 733 (2023).
- [14] J. D. Fletcher, W. Park, S. Ryu, P. See, J. P. Griffiths, G. A. C. Jones, I. Farrer, D. A. Ritchie, H.-S. Sim, and M. Kataoka, Time-resolved Coulomb collision of single electrons, *Nat. Nanotech.* **18**, 727 (2023).
- [15] J. Wang, H. Edlbauer, A. Richard, S. Ota, W. Park, J. Shim, A. Ludwig, A. D. Wieck, H.-S. Sim, M. Urdampilleta, T. Meunier, T. Kodera, N.-H. Kaneko, H. Sellier, X. Waintal, S. Takada, and C. Bäuerle, Coulomb-mediated antibunching of an electron pair surfing on sound, *Nat. Nanotech.* **18**, 721 (2023).
- [16] S. Giblin, M. Kataoka, J. Fletcher, P. See, T. Janssen, J. Griffiths, G. Jones, I. Farrer, and D. Ritchie, Towards a quantum representation of the ampere using single electron pumps, *Nat. Commun.* **3**, 930 (2012).
- [17] M. Aluffi, T. Vasselon, S. Ouacel, H. Edlbauer, C. Geffroy, P. Rouleau, D. C. Glattli, G. Georgiou, and C. Bäuerle, Ultrashort electron wave packets via frequency-comb synthesis, *Phys. Rev. Appl.* **20**, 034005 (2023).
- [18] M. Acciai, F. Ronetti, D. Ferraro, J. Rech, T. Jonckheere, M. Sasseti, and T. Martin, Levitons in superconducting point contacts, *Phys. Rev. B* **100**, 085418 (2019).
- [19] F. Ronetti, M. Carrega, and M. Sasseti, Levitons in helical liquids with Rashba spin-orbit coupling probed by a superconducting contact, *Phys. Rev. Research* **2**, 013203 (2020).
- [20] P. Buset, B. Roussel, M. Moskalets, and C. Flindt, Tunable Andreev-Conversion of Single-Electron Charge Pulses, [arXiv:2312.13145](https://arxiv.org/abs/2312.13145) (2023).
- [21] P. Buset, B. Roussel, M. Moskalets, and C. Flindt, Floquet-Nambu theory of electron quantum optics with superconductors, in prep.
- [22] W. Belzig and M. Vanevic, Elementary Andreev processes in a driven superconductor-normal metal contact, *Physica E* **75**, 22 (2016).
- [23] D. V. Averin, G. Wang, and A. S. Vasenko, Time-dependent Andreev reflection, *Phys. Rev. B* **102**, 144516 (2020).
- [24] B. Bertin-Johannet, J. Rech, T. Jonckheere, B. Grémaud, L. Raymond, and T. Martin, Microscopic theory of photoassisted electronic transport in normal-metal/BCS-superconductor junctions, *Phys. Rev. B* **105**, 115112 (2022).
- [25] B. Bertin-Johannet, B. Grémaud, F. Ronetti, L. Raymond, J. Rech, T. Jonckheere, and T. Martin, Current and shot noise in a normal metal-superconductor junction driven by spin-dependent periodic pulse sequence, *Phys. Rev. B* **109**, 174514 (2024).
- [26] J. Eroms, D. Weiss, J. D. Boeck, G. Borghs, and U. Zülicke, Andreev Reflection at High Magnetic Fields: Evidence for Electron and Hole Transport in Edge States, *Phys. Rev. Lett.* **95**, 107001 (2005).
- [27] I. E. Batov, T. Schäpers, N. M. Chtchelkatchev, H. Hardtdegen, and A. V. Ustinov, Andreev reflection and strongly enhanced magnetoresistance oscillations in $\text{Ga}_x\text{In}_{1-x}\text{As}/\text{InP}$ heterostructures with superconducting contacts, *Phys. Rev. B* **76**, 115313 (2007).
- [28] P. Rickhaus, M. Weiss, L. Marot, and C. Schönberger, Quantum Hall Effect in Graphene with Superconducting Electrodes, *Nano Lett.* **12**, 1942 (2012).
- [29] Z. Wan, A. Kazakov, M. J. Manfra, L. N. Pfeiffer, K. W. West, and L. P. Rokhinson, Induced superconductivity in high-mobility two-dimensional electron gas in gallium arsenide heterostructures, *Nat. Commun.* **6**, 1 (2015).
- [30] V. E. Calado, S. Goswami, G. Nanda, M. Diez, A. R. Akhmerov, K. Watanabe, T. Taniguchi, T. M. Klapwijk, and L. M. K. Vandersypen, Ballistic Josephson junctions in edge-contacted graphene, *Nat. Nanotech.* **10**, 761 (2015).
- [31] M. Ben Shalom, M. J. Zhu, V. I. Fal'ko, A. Mishchenko, A. V. Kretinin, K. S. Novoselov, C. R. Woods, K. Watanabe, T. Taniguchi, A. K. Geim, and J. R. Prance, Quantum oscillations of the critical current and high-field superconducting proximity in ballistic graphene, *Nat. Phys.* **12**, 318 (2016).
- [32] F. Amet, C. T. Ke, I. V. Borzenets, J. Wang, K. Watanabe, T. Taniguchi, R. S. Deacon, M. Yamamoto, Y. Bomze, S. Tarucha, and G. Finkelstein, Supercurrent in the quantum Hall regime, *Science* **352**, 966 (2016).
- [33] G.-H. Lee, K.-F. Huang, D. K. Efetov, D. S. Wei, S. Hart, T. Taniguchi, K. Watanabe, A. Yacoby, and P. Kim, Inducing superconducting correlation in quantum Hall edge states, *Nat. Phys.* **13**, 693 (2017).
- [34] M. R. Sahu, X. Liu, A. K. Paul, S. Das, P. Raychaudhuri, J. K. Jain, and A. Das, Inter-Landau-level Andreev Reflection at the Dirac Point in a Graphene Quantum Hall State Coupled to a NbSe_2 Superconductor, *Phys. Rev. Lett.* **121**, 086809 (2018).
- [35] L. Zhao, E. G. Arnault, A. Bondarev, A. Serebinski, T. F. Q. Larson, A. W. Draelos, H. Li, K. Watanabe, T. Taniguchi, F. Amet, H. U. Baranger, and G. Finkelstein, Interference of chiral Andreev edge states, *Nat. Phys.* **16**, 862 (2020).
- [36] M. R. Sahu, A. K. Paul, J. Sutradhar, K. Watanabe, T. Taniguchi, V. Singh, S. Mukerjee, S. Banerjee, and A. Das, Quantized conductance with nonzero shot noise as a signature of Andreev edge state, *Phys. Rev. B* **104**, L081404 (2021).
- [37] M. Hatefipour, J. J. Cuzzo, J. Kanter, W. M. Strickland, C. R. Allemang, T.-M. Lu, E. Rossi, and J. Shabani, Induced superconducting pairing in integer quantum Hall edge states, *Nano Lett.* **22**, 6173 (2022).
- [38] H. Vignaud, D. Perconte, W. Yang, B. Kousar, E. Wagner, F. Gay, K. Watanabe, T. Taniguchi, H. Courtois, Z. Han, H. Sellier, and B. Sacépé, Evidence for chiral supercurrent in quantum hall Josephson junctions, *Nature* **624**, 545–550 (2023).
- [39] L. Zhao, Z. Iftikhar, T. F. Q. Larson, E. G. Arnault, K. Watanabe, T. Taniguchi, F. Amet, and G. Finkelstein, Loss and Decoherence at the Quantum Hall-Superconductor Interface, *Phys. Rev. Lett.* **131**, 176604 (2023).
- [40] D. J. Clarke, J. Alicea, and K. Shtengel, Exotic cir-

- cuit elements from zero-modes in hybrid superconductor-quantum-Hall systems, *Nat. Phys.* **10**, 877 (2014).
- [41] X.-L. Huang and Y. V. Nazarov, Supercurrents in Unidirectional Channels Originate from Information Transfer in the Opposite Direction: A Theoretical Prediction, *Phys. Rev. Lett.* **118**, 177001 (2017).
- [42] X.-L. Huang and Y. V. Nazarov, Interaction-induced supercurrent in quantum Hall setups, *Phys. Rev. B* **100**, 155411 (2019).
- [43] S.-B. Zhang and B. Trauzettel, Perfect Crossed Andreev Reflection in Dirac Hybrid Junctions in the Quantum Hall Regime, *Phys. Rev. Lett.* **122**, 257701 (2019).
- [44] A. L. R. Manesco, I. M. Flór, C.-X. Liu, and A. R. Akhmerov, Mechanisms of Andreev reflection in quantum Hall graphene, *SciPost Phys. Core* **5**, 045 (2022).
- [45] T. H. Galambos, F. Ronetti, B. Hetényi, D. Loss, and J. Klinovaja, Crossed Andreev reflection in spin-polarized chiral edge states due to the Meissner effect, *Phys. Rev. B* **106**, 075410 (2022).
- [46] V. D. Kurilovich, Z. M. Raines, and L. I. Glazman, Disorder-enabled Andreev reflection of a quantum Hall edge, *Nat. Commun.* **14**, 1 (2023).
- [47] A. B. Michelsen, P. Recher, B. Braunecker, and T. L. Schmidt, Supercurrent-enabled Andreev reflection in a chiral quantum Hall edge state, *Phys. Rev. Res.* **5**, 013066 (2023).
- [48] N. Schiller, B. A. Katzir, A. Stern, E. Berg, N. H. Lindner, and Y. Oreg, Superconductivity and fermionic dissipation in quantum hall edges, *Phys. Rev. B* **107**, L161105 (2023).
- [49] L. Arrachea, A. L. Yeyati, and C. A. Balseiro, Signatures of triplet superconductivity in $\nu = 2$ chiral Andreev states, *Phys. Rev. B* **109**, 064519 (2024).
- [50] D. Dasenbrook and C. Flindt, Dynamical generation and detection of entanglement in neutral leviton pairs, *Phys. Rev. B* **92**, 161412 (2015).
- [51] V. Kashcheyevs, P. Degiovanni, B. Roussel, M. Kataoka, F. J. D., L. Freise, N. Ubbelohde, G. Fève, H. Bartolomei, F. Couedo, A. Kadykov, W. Poirier, P. Roulleau, F. D. Parmentier, and F. Hohls, *Single-electron wave packets for quantum metrology: concepts, implementations, and applications*, White paper (2022).
- [52] D. Ferraro, A. Feller, A. Ghibaudo, E. Thibierge, E. Bocquillon, G. Fève, C. Grenier, and P. Degiovanni, Wigner function approach to single electron coherence in quantum Hall edge channels, *Phys. Rev. B* **88**, 205303 (2013).
- [53] D. Ferraro, B. Roussel, C. Cabart, E. Thibierge, G. Fève, C. Grenier, and P. Degiovanni, Real-Time Decoherence of Landau and Leviton Quasiparticles in Quantum Hall Edge Channels, *Phys. Rev. Lett.* **113**, 166403 (2014).
- [54] B. Roussel, C. Cabart, G. Fève, and P. Degiovanni, Processing Quantum Signals Carried by Electrical Currents, *PRX Quantum* **2**, 020314 (2021).
- [55] G. E. Blonder, M. Tinkham, and T. M. Klapwijk, Transition from metallic to tunneling regimes in superconducting microconstrictions: Excess current, charge imbalance, and supercurrent conversion, *Phys. Rev. B* **25**, 4515 (1982).
- [56] M. Sigrist and K. Ueda, Phenomenological theory of unconventional superconductivity, *Rev. Mod. Phys.* **63**, 239 (1991).
- [57] J. Kotilahti, P. Buset, M. Moskalets, and C. Flindt, Multi-particle interference in an electronic Mach-Zehnder interferometer, *Entropy* **23**, 736 (2021).
- [58] G. Haack, M. Moskalets, and M. Büttiker, Glauber coherence of single-electron sources, *Phys. Rev. B* **87**, 201302 (2013).
- [59] M. Moskalets, First-order correlation function of a stream of single-electron wave packets, *Phys. Rev. B* **91**, 195431 (2015).
- [60] M. Moskalets and G. Haack, Single-electron coherence: Finite temperature versus pure dephasing, *Physica E* **75**, 358 (2016).
- [61] M. Moskalets, Fractionally Charged Zero-Energy Single-Particle Excitations in a Driven Fermi Sea, *Phys. Rev. Lett.* **117**, 046801 (2016).
- [62] M. Moskalets, J. Kotilahti, P. Buset, and C. Flindt, Composite two-particle sources, *Eur. Phys. J. Spec. Top.* **229**, 647 (2020).
- [63] P. Flandrin, *Time-frequency/time-scale analysis* (Academic press, 1998).
- [64] R. Landauer and T. Martin, Barrier interaction time in tunneling, *Rev. Mod. Phys.* **66**, 217 (1994).
- [65] H. G. Winful, Tunneling time, the Hartman effect, and superluminality: A proposed resolution of an old paradox, *Phys. Rep.* **436**, 1 (2006).
- [66] H. Y. Yao, N. C. Chen, T. H. Chang, and H. G. Winful, Frequency-dependent cavity lifetime and apparent superluminality in Fabry-Pérot-like interferometers, *Phys. Rev. A* **86**, 053832 (2012).
- [67] L. S. Levitov, H. Lee, and G. B. Lesovik, Electron counting statistics and coherent states of electric current, *J. Math. Phys.* **37**, 4845 (1996).
- [68] D. A. Ivanov, H. W. Lee, and L. S. Levitov, Coherent states of alternating current, *Phys. Rev. B* **56**, 6839 (1997).
- [69] I. Safi, A dynamic scattering approach for a gated interacting wire, *The European Physical Journal B-Condensed Matter and Complex Systems* **12**, 451 (1999).
- [70] J. Keeling, I. Klich, and L. S. Levitov, Minimal Excitation States of Electrons in One-Dimensional Wires, *Phys. Rev. Lett.* **97**, 116403 (2006).
- [71] N. Dashti, M. Misiorny, S. Kheradsoud, P. Samuelsson, and J. Splettstoesser, Minimal excitation single-particle emitters: Comparison of charge-transport and energy-transport properties, *Phys. Rev. B* **100**, 035405 (2019).
- [72] M. V. Moskalets, *Scattering Matrix Approach to Non-Stationary Quantum Transport* (Imperial College Press, 2011).
- [73] P. Pandey, R. Danneau, and D. Beckmann, Ballistic Graphene Cooper Pair Splitter, *Phys. Rev. Lett.* **126**, 147701 (2021).
- [74] G. Wang, T. Dvir, G. P. Mazur, C.-X. Liu, N. van Loo, S. L. D. ten Haaf, A. Bordin, S. Gazibegovic, G. Badawy, E. P. A. M. Bakkers, M. Wimmer, and L. P. Kouwenhoven, Singlet and triplet Cooper pair splitting in hybrid superconducting nanowires, *Nature* **612**, 448 (2022).
- [75] A. Bordoloi, V. Zannier, L. Sorba, C. Schönenberger, and A. Baumgartner, Spin cross-correlation experiments in an electron entangler, *Nature* **612**, 454 (2022).
- [76] B. Bertin-Johannet, L. Raymond, F. Ronetti, J. Rech, T. Jonckheere, B. Grémaud, and T. Martin, An on-demand source of energy-entangled electrons using levitons, *Appl. Phys. Lett.* **122**, 202601 (2023).